PHYSICAL REVIEW B VOLUME 48, NUMBER 14 1 OCTOBER 1993-II

Hyperfine interactions of ^{111}Cd in Ga_2O_3

A. F. Pasquevich
Departamento de Fisica, Universidad Nacional de La Plata, c.c. No. 67, 1900 La Plata, Argentina

M. Uhrmacher, L. Ziegeler, and K. P. Lieb
II. Physikalisches Institut Universität Göttingen, Bunsenstrasse 7–9, 37073 Göttingen, Germany
(Received 23 November 1992; revised manuscript received 26 March 1993)

Perturbed-angular-correlation measurements were carried out after implantation of ^{111}In into amorphous and polycrystalline powder samples of α- and β-Ga_2O_3, and single crystals of β-Ga_2O_3. After annealing of the radiation damage the quadrupole hyperfine interactions of ^{111}Cd were determined. In both α- and β-crystalline phases, three electric-quadrupole interactions were observed. In addition, the orientations of the electric-field gradients in β-Ga_2O_3 at the probe sites were determined. In β-Ga_2O_3 preferential substitutional In occupation of the octahedral sites was found. Two of the quadrupole interactions in α- and β-Ga_2O_3 are attributed to different charge states of the ^{111}Cd impurity (Cd^0) and (Cd^-). Their populations varied in a reversible way in the temperature range 450–700 K and also can be influenced by the oxygen pressure.

I. INTRODUCTION

In the last few years the time-differential perturbed-angular-correlation technique (PAC) has been extensively applied to study the hyperfine interactions of $^{111}In(EC)^{111}Cd$ as impurities in metal oxides. These investigations served two purposes: The possibility to study the electric-field gradient (EFG) of the Cd-O bond in terms of the crystallographic structure of the host material[1] has been explored. Recently, an indication of mainly ionic bonds for Cd in the octahedral sites of oxides with bixbyite structure has been inferred from the scaling of the EFG with the lattice constant.[2] Furthermore, the common way of introducing the hyperfine probe ^{111}Cd into the host by electron capture decay of ^{111}In allows the investigation of the interaction between impurities and electronic defects. Dynamic effects during the relaxation of the probe's electronic system have been correlated with the electronic properties of the impurity-host system.[3] In semiconducting oxides the possibility of hyperfine interactions from localized electron holes must be considered. A similar idea has been discussed in connection with Cd centers in elemental and III-V semiconductors.[4]

The present study is mainly devoted to the hyperfine interactions of ^{111}Cd in β-Ga_2O_3 and fits well in the framework mentioned above. This oxide with monoclinic lattice symmetry offers both fourfold and sixfold oxygen coordinated cation sites. In a recent PAC study on ^{111}In probes in β-Ga_2O_3 in which the radioactive tracer was introduced chemically, ^{111}In was found to replace Ga at the sixfold coordinated one.[5]

We now report on PAC experiments after ^{111}In implantation. We hoped to overcome the chemical preference for one site by that technique. Unavoidably, radiation damage is produced during implantation which has to be removed by annealing the sample and thus may change the distribution of the implanted impurities. Furthermore, heavy ion irradiation can turn a semiconducting host amorphous and this part of the sample might crystallize to a different phase during annealing.[6] Although the doses used in typical PAC experiments are much smaller than those necessary for completely amorphizing of the sample, the PAC technique sensitively detects the presence of submicroscopic regions of other phases. For that reason, although the paper is mainly devoted to the annealing behavior and the temperature dependence of the hyperfine interactions of ^{111}Cd in β-Ga_2O_3, PAC experiments are also reported in the amorphous and the α form of Ga_2O_3.

Numerous PAC experiments in single crystals have been carried out over the last years to study defects and defect-impurity interactions in hosts of cubic symmetry, like metals, elemental semiconductors, and III-V compounds.[4] Measurements in single-crystalline ionic compounds have been carried out less frequently.[7,8] PAC measurements on single crystals provide a direct correlation between the directions of the crystallographic axes and the principal axes of the EFG tensor.[9]

In the present paper, the EFG of ^{111}Cd on sites in Ga_2O_3 is analyzed in terms of lattice structure, site location, temperature, and oxygen pressure during measurements in the polycrystalline, single-crystalline, and amorphous forms mentioned before.

II. GALLIUM OXIDE PROPERTIES

The binary oxides of Ga are similar to those of Al but have been studied in less detail. Gallium sesquioxide exists in several crystalline forms: α, β, γ, δ, and ϵ. Figure 1 illustrates the phase transformations among the different forms and also its hydrates.[10] β-Ga_2O_3 is

0163-1829/93/48(14)/10052(11)/$06.00

the most stable crystalline modification. It has a monoclinic structure with the oxygen ions arranged in a distorted cubic closed packed lattice and the Ga ions at the distorted tetrahedral and octahedral sites[11] as shown in Fig. 1. The unit cell contains four molecules and has the lattice parameters a=12.23 Å, b=3.04 Å, c=5.80 Å, and β=103.7°. Optical,[12,13] magnetic,[14] and hyperfine properties[15] of β-Ga_2O_3 have been reported. At 295 K, the optical energy gap for β-Ga_2O_3 films was determined to be 4.23 eV.[12] Because of this large gap, an electronic behavior similar to the one reported for Cd-doped In_2O_3 (Ref. 3) can be expected.

Data on α-Ga_2O_3 (corundum type) are more scarce. The corundum structure is a distorted hexagonal closed packed array of oxygen ions with 2/3 of the cations on octahedral sites. The unit cell contains two molecules and is defined by[16] a=5.32 Å and α=55.8°. In Co-doped α-Ga_2O_3 films an optical energy gap of 2.41 eV has been reported.[12]

III. EXPERIMENTAL PROCEDURES AND ANALYSIS

A. Sample preparation

Gallium oxide was prepared using high-purity gallium metal (99.9999%) and high-purity nitric and hydrochloric acid and ammonia.

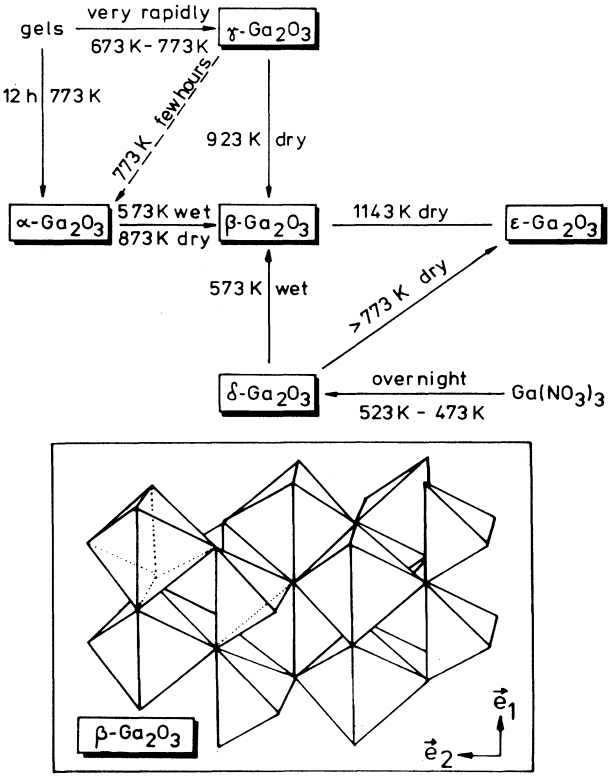

FIG. 1. In the upper part the transformation relationships among the forms of gallium oxide and its hydrates are shown. Below a perspectivic view of the arrangement of the oxygen octahedra and tetrahedra in β-Ga_2O_3 is given. The crystal axes are indicated.

β–Ga_2O_3. Ga was dissolved in HNO_3. After evaporation of the acid, the remaining $Ga(NO_3)_3$ was dried and heated up to 1173 K in a quartz crucible. An x-ray diffraction analysis of this polycrystalline powder showed Ga_2O_3 in its pure β-form. The single crystals were flux grown in the Philips Forschungslabor Hamburg and were analyzed by Harms.[17] The crystallographic orientation was determined by Laue analysis. The crystals had the form of slabs and the face with the largest surface was normal to the monoclinic b axis.

α–Ga_2O_3. The Ga metal was dissolved in a 1:1 mixture of HNO_3 and HCl. The acid solution was heated and the precipitate of $Ga(OH)_3$ was formed by adding a NH_3-solution until pH = 8 was reached. After centrifugation and washing, the wet precipitate was slowly heated up to 753 K and kept at this temperature for 12 h. This procedure yielded α-Ga_2O_3, as was again confirmed by x-ray analysis.

Amorphous Ga_2O_3. Ga was dissolved in HNO_3. After evaporation of the acid, the remaining $Ga(NO_3)_3$ was slowly heated to 523 K and kept at this temperature for 12 h. x-ray diffraction analysis did not show any diffraction line pattern.

B. Implantation

The polycrystalline oxide powders were rolled onto Ag foils. The samples were implanted with 400 keV ^{111}In ions to a total amount of 10^{12} ions at the Göttingen heavy ion implantor IONAS.[18] The mean range of the implanted ions was about 90 nm with an estimated maximum concentration of less than 10^{-2} at. %. In the case of the β-Ga_2O_3 single crystal, the implantation was carried out along the monoclinic b axis.

C. PAC measurements

1. Polycrystalline samples

Annealings at a given temperature were carried out for 2 h before starting the PAC measurement at the same temperature. The cases where the annealing temperature T_a was different from the measurement temperature T_m will be marked in the text. Annealings took place in open air (1 atm). The PAC spectra were taken with a set-up of four NaI(Tl) detectors arranged in 90° geometry.[19] $R(t)$ perturbation functions were determined from the 12 simultaneously measured PAC spectra and then Fourier transformed as described elsewhere.[19]

For a static quadrupole interaction in a polycrystalline sample the perturbation factor has the form[20]

$$G_2^{\mathrm{st}}(t) = \sum_{n=0}^{3} S_{2n}(\eta)\cos(\omega_n t)e^{-\delta\omega_n t}, \qquad (1)$$

where the superscript st denotes the static character of the interaction. The frequencies ω_n are related to the quadrupole frequency $\nu_Q = eQV_{zz}/h$ by $\omega_n = g_n(\eta)\nu_Q$. The coefficients g_n and S_{2n} are known functions[20] of the asymmetry parameter $\eta = (V_{xx} - V_{yy})/V_{zz}$, where V_{ii}

denote the principal components of the EFG tensor. The exponential factor accounts for a Lorentzian frequency distribution with a relative width δ around ω_n.

In the presence of a fluctuating EFG, the perturbation factor is damped with time and the simple expression

$$G_2^{\mathrm{dyn}}(t) = e^{-\lambda_2 t} G_2^{\mathrm{st}} \tag{2}$$

holds in the case of slow relaxation.[21]

To consider the possibility of several surroundings (labeled i) of the probe nuclei, a superposition of up to three perturbation factors weighted with their relative fractions f_i was assumed:

$$G_2(t) = \sum_{i=1}^{\leq 5} f_i G_{2,i}^{x}(t) \quad (x = \mathrm{st}, \mathrm{dyn}). \tag{3}$$

2. *Single-crystalline samples*

In order to obtain the electric-quadrupole interaction parameters from the PAC measurement, the 12 spectra were combined, as it is usually done for polycrystalline samples. But in the perturbation factor [Eq. (1)] the coefficients S_{2n} depend now on the asymmetry parameter η and on the angles between the direction $\mathbf{k_i}$ of the emission of the two γ-rays and the principal axis of the EFG tensor.[9] To fit the experimental data, the possibility of several EFG fractions was again taken into account.

The different crystal orientations relative to the four detectors are defined in the following way: Z is the axis normal to the detector plane and X and Y are along the lines which join opposite detectors. The spectra taken at different crystal orientations are labeled with the polar coordinates (Θ_2, Φ_2) and (Θ_3, Φ_3) of the two crystallographic vectors $\mathbf{e_2}$ and $\mathbf{e_3}$, with respect to the laboratory system XYZ defined before. $\mathbf{e_2}$ was taken along the monoclinic direction a, and $\mathbf{e_3}$ was taken along the $(b \times a)$ axis. The angle Φ_i is undefined whenever Θ_i=0; these cases have been labeled with the letter u. The orientation of the single crystals during the high-temperature measurements could be affected by errors of a few degrees ($\leq 5°$) since the geometry of the oven did not allow the use of a goniometer.

IV. RESULTS

A. Polycrystalline β-Ga_2O_3 samples

The thermal annealing behavior of the radiation damage was studied first. The spectra behave in a predictable way: the radiation damage produces a broad EFG distribution in the as-implanted sample and sharp interactions appear with increasing annealing temperature T_a. After a 2-hour annealing at 1073 K, the quadrupole interactions of ^{111}In(EC)^{111}Cd in β–Ga_2O_3 are well defined, especially if they are measured at high temperatures ($T_m \geq$ 600 K).

The temperature dependence of the quadrupole interaction was studied between room temperature and T_m= 800 K. Typical spectra obtained at normal pressure (1 atm) are shown in Fig. 2. The experiment was then repeated at 2×10^{-5} mbar and gave similar spectra. As observed in several ionic oxides with sixfold oxygen coordination, the spectra get much sharper at higher measuring temperature.[2,22] Three hyperfine interaction fractions are sufficient to fit the data, the parameters are summarized in Table I.

In Fig. 3 the temperature dependence of the EFG parameters measured at both oxygen pressures is displayed. The most relevant aspects are the following.

(a) The quadrupole frequencies are essentially constant as a function of the oxygen pressure and the measurement temperature. All EFG parameters connected to the component I_3 are constant.

(b) Strong variations are found for the fractions f_1 and f_2, which exchange their values at $T_c \approx 650$ K (normal pressure) and $T_c \approx 580$ K (at 2×10^{-5} mbar).

(c) There are pronounced changes of η_2 and δ_2 with temperature: both parameters decrease with increasing T_m at both oxygen pressures. However, some caution is necessary in this case, as simultaneously fraction f_2 decreases to zero and the fit becomes less sensitive.

(d) Between 450 K and 570 K, a slow relaxation affects the interactions I_1 and I_3. The perturbation factors corresponding to these components were modulated as indicated in Eq. (2). The relaxation constant λ_2 changed with temperature, but was assumed to be the same for both components. Its maximum value was $\lambda_2 = 9 \times 10^6$ s^{-1} at 500 K.

B. Single-crystalline β-Ga_2O_3 samples

In general, the same behavior was observed in the case of the β-Ga_2O_3 single crystal. Annealings up to T_a =

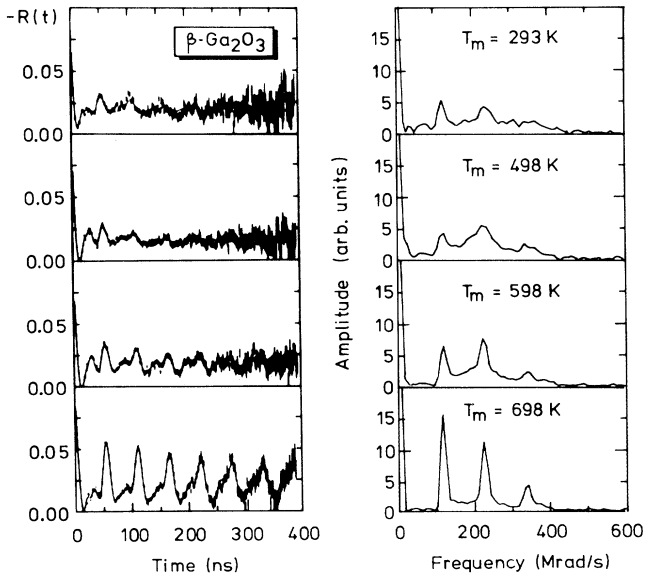

FIG. 2. PAC spectra and their Fourier transforms for ^{111}Cd in polycrystalline β-Ga_2O_3 (after removal of radiation damage) as a function of the measuring temperature T_m under normal pressure.

TABLE I. Electric-quadrupole interaction parameters of ^{111}Cd in the oxides α-Ga_2O_3 and β-Ga_2O_3 measured at two different temperatures.

Matrix	T_m(K)	f_i (%)	ν_Q(MHz)	η	δ (%)	A_{22}
β-Ga_2O_3	293	1: 26(1)	124.1(6)	0.17(2)	6(1)	0.09
		2: 54(2)	145(5)	0.78(5)	46(4)	
		3: 13(1)	191(3)	0.53(4)	13(2)	
	793	1: 65(2)	119.6(1)	0.13(1)	1(1)	0.10
		2: 13(3)	135(4)	0.20(4)	6(2)	
		3: 22(2)	180(3)	0.33(2)	12(2)	
β-Ga_2O_3, single crystal	863	1: 69(1)	119.1(1)	0.13(1)	<1(1)	0.12
		2: 11(1)	138(1)	0.32(1)	4(1)	
		3: 20(1)	184(1)	0.32(6)	12(2)	
α-Ga_2O_3	293	1: 2(2)	182(2)	0	1(1)	0.08
		2: 58(5)	111(8)	0.9(3)	27(3)	
		3: 40(5)	195(3)	0.7(1)	9(5)	
	723	1: 31(2)	180(1)	0	1(1)	0.09
		2: 30(5)	113(8)	0.67(9)	19(3)	
		3: 39(1)	196(2)	0.59(3)	11(1)	

1073 K were carried out in air. The PAC spectra and their Fourier transforms were fitted with the characteristic three interactions I_1, I_2, and I_3 deduced in the polycrystalline samples.

In the case of the single-crystalline sample the analysis of PAC data is more complex.[7,9] Especially the coefficients S_{2n} of Eq. (1) depend on the orientation of the EFG-axes (x, y, z) relative to the detector positions. To avoid a free-fitting procedure which often gives unstable solutions due to the large number of parameters, we decided on a different strategy: We chose the PAC spectrum which showed the main hyperfine interaction I_1 well defined with a large fraction ($\approx 70\%$) and estimated the S_{2n} values from its Fourier amplitudes. Then the parameters for the three quadrupole interactions were fitted as free parameters, assuming that the interactions I_1 and I_2 had the same S_{2n} coefficients. In fact, this is true only at high measuring temperatures ($T_m \geq T_c$) as shown later. At $T_m \leq T_c$ the interaction I_2 is broadly distributed hiding any effect of the single-crystalline sample. Furthermore,

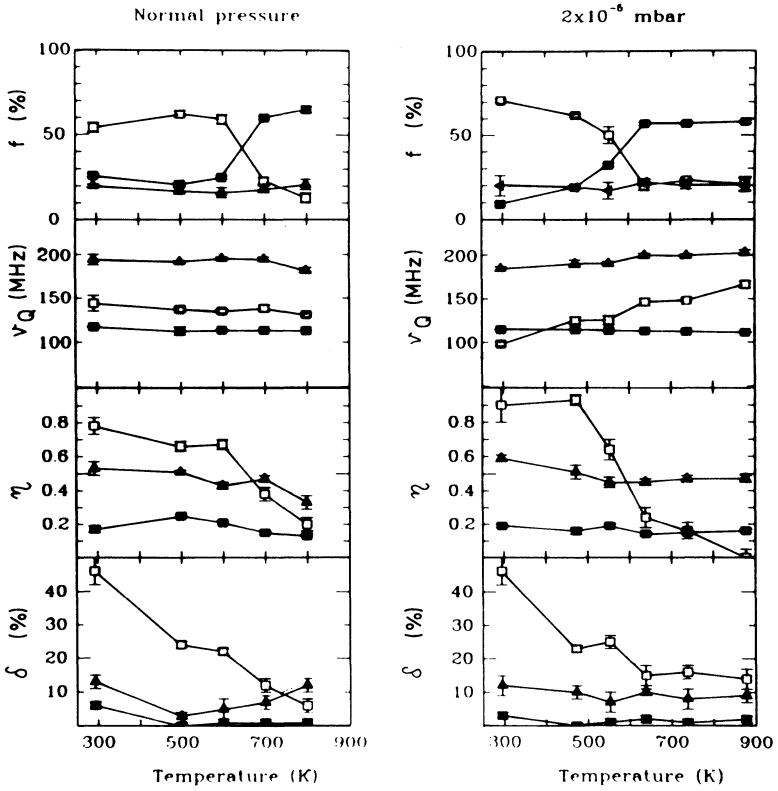

FIG. 3. Values of the hyperfine parameters as a function of the measurement temperature for both air pressures used: normal pressure (left) and 2.0×10^{-5} mbar (right). The symbols ■, □, and ▲ correspond to the interactions labeled I_1, I_2 and I_3.

the fraction I_3 was treated as in the polycrystalline material, due to its large distribution width δ_3 and its small fraction f_3.

PAC results for different crystal orientations are displayed in Fig. 4. In addition to the angles defining the crystal orientation the insets in Fig. 4 show the orientation of the axes $\mathbf{e_2}$ and $\mathbf{e_3}$ relative to the detectors. All measurements were done at $830 \leq T_m \leq 870$ K. These PAC spectra were fitted with a fixed set of quadrupole parameters and only the S_{2n} coefficients for I_1 and I_2 were adjusted for each crystal orientation. The S_{2n} coefficients obtained are summarized in Table II. Two results of Fig. 4 are obvious: (a) the Fourier peak assigned to I_2 — clearly seen in Fig. 4(c) — shows the same orientation dependence as I_1 and (b) for $\mathbf{e_3}$ pointing to any detector, a higher S_{20} value is obtained.

After annealing the single crystal at $T_a = 1073$ K, we measured the temperature dependence of the EFG's. The PAC spectra are given in Fig. 5. At the different temperatures we used the following set of S_{2n} coefficients: $S_{20} = 0$, $S_{21} = 0.89$, $S_{22} = 0$, $S_{23} = 0.11$. The dependence of the hyperfine parameters is displayed in Fig. 6. The major aspects found in the polycrystalline material are again observed.

C. Polycrystalline α-Ga_2O_3 samples

Experiments in α-Ga_2O_3 were carried out in a way similar to the one reported for the β form but without the low-pressure investigation. After annealing the samples at the highest temperature possible without changing them to the β phase, the temperature dependence of the hyperfine interactions was studied (Fig. 7). Again three interactions were required to fit the data; typical values of the EFG parameters are given in Table I. As the spectra sensitively depend on the temperature, results at different T_m values are included. The temperature de-

TABLE II. Coefficients S_{2n} determined for interactions I_1 and I_2 for different crystal orientations at $T_m \geq 830$ K. The calculated values assuming that the EFG axes are along the crystallographic directions $(\mathbf{e_1}, \mathbf{e_2}, \mathbf{e_3})$ are also tabulated.

Orientation	I_i	S_{20}	S_{21}	S_{22}	S_{23}
	I_1	0	0.86	0.01	0.13
$(90°, 45°, 0°, u)$	I_2	0	0.95	0.02	0.03
	Calc:	0	0.95	0	0.05
	I_1	0.10	0.79	0.01	0.10
$(90°, 0°, 0°, u)$	I_2	0	0.95	0.02	0.03
	Calc:	0.03	0.91	0	0.06
	I_1	0.65	0.20	0.03	0.02
$(0°, u, 90°, 0°)$	I_2	0.61	0.27	0.02	0
	Calc:	0.72	0.25	0.01	0.02
	I_1	0.71	0.22	0.05	0.02
(90°,-90°,90°,0°)	I_2	0.57	0.29	0.13	0.01
	Calc:	0.79	0.21	0	0
	I_1	0	0.20	0.80	0.0
(90°,-45°,90°,45°)	I_2	0.55	0.14	0.31	0
	Calc:	0	0.21	0.75	0.04

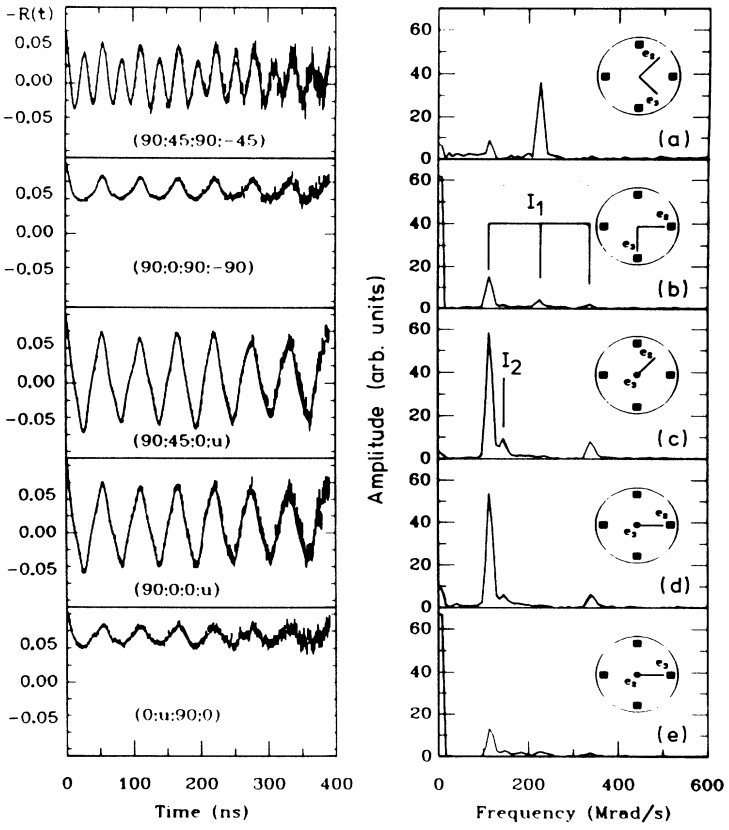

FIG. 4. PAC spectra and Fourier transforms of ^{111}In implanted in the β-Ga_2O_3 single crystal taken at different crystal orientations. The figures are marked with the angles between the crystallographic vectors $\mathbf{e_2}$ and $\mathbf{e_3}$ and the detector axes XYZ. The insets in the figures show the orientation of $\mathbf{e_2}$ and $\mathbf{e_3}$ relative to the detectors (dots) in the XY plane. A central dot indicates that one of these vectors is normal to the XY plane. The temperature T_m was always in the range 830 – 870 K.

pendence is similar to the one found in the case of the β form. Here the transition between I_1 and I_2 occurs at $T_c \approx 580$ K, after annealing at $T_a = 773$ K. This is shown in Fig. 8, where the fitted fraction f_1 of the interaction I_1 is displayed. Above T_c, f_2 transformed to f_1, while f_3 stayed nearly constant (40%). Annealing to 833 K produced the PAC spectra typical for the β form, thus indicating the structural phase transition.

D. Amorphous Ga_2O_3

The spectrum obtained directly after implantation [Fig. (9a)] was similar to the one reported for the β form as implanted. Both correspond to a broad frequency distribution which involves about 80% of the probes, their quadrupole parameters being $\nu_Q = 172(6)$ MHz, $\eta \approx 0.9$, and $\delta_Q = 26$–$40\,\%$. There was an additional small fraction (16%) with EFG parameters of the interaction we observed in β-Ga_2O_3 after removal of the radiation damage and aging the sample for several days at room temperature. The spectra kept this structure after annealing the sample at 673 K, in agreement with the results reported in Ref. 5. The measurement at 783 K [Fig. (9a)] showed the interactions characteristic of β-Ga_2O_3, but corresponding to a lower measurement temperature (see Fig. 2). After annealing at 1123 K, a measurement $T_m = 783$ K showed the well-defined interaction I_1 typical for β-Ga_2O_3. No evidence of the ϵ phase was found.

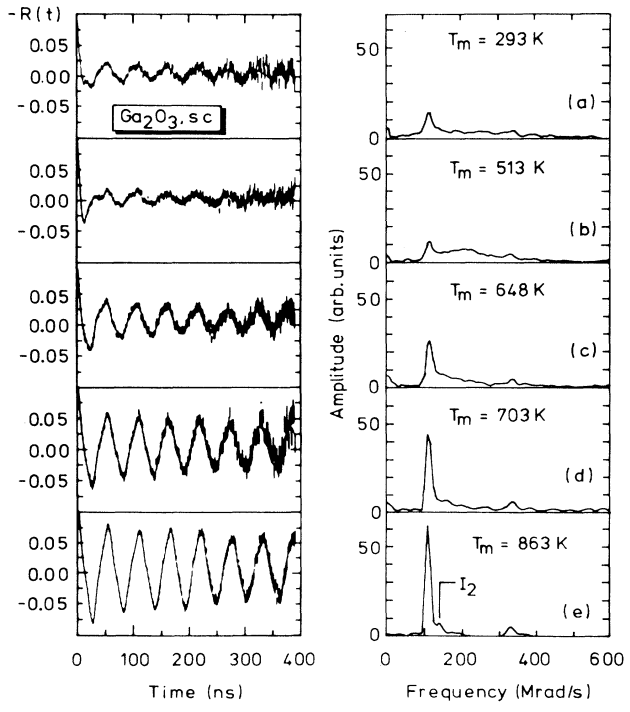

FIG. 5. PAC spectra and their Fourier transforms at different measuring temperatures T_m after annealing the β-Ga_2O_3 single crystal at $T_a = 1073$ K.

V. DISCUSSION

We have seen that the hyperfine interaction of ^{111}Cd nuclei in different crystalline forms of Ga_2O_3, after ^{111}In ion implantation and nuclear decay by electron capture, is characterized by three electric-field gradients which depend on the crystalline structure of the host, the temperature, the thermal history, and to some extent on the oxygen pressure. We will now interpret these results according to the lattice structure and consider possible modifications of the charge distribution taking place near the probe atom. In doing so we will compare our results with the ones obtained via PAC and Mössbauer spectroscopy in related oxides. We will first discuss β-Ga_2O_3 considering the site location and the charge state of the probes. We then will discuss α-Ga_2O_3 and the amorphous form of gallium oxide.

A. Site location

The present ^{111}In implantation experiments confirm the dominant hyperfine interaction (I_1) for ^{111}Cd in β-Ga_2O_3 which was already observed in chemically prepared samples.[5] As found in many binary oxides[1,2,22] the

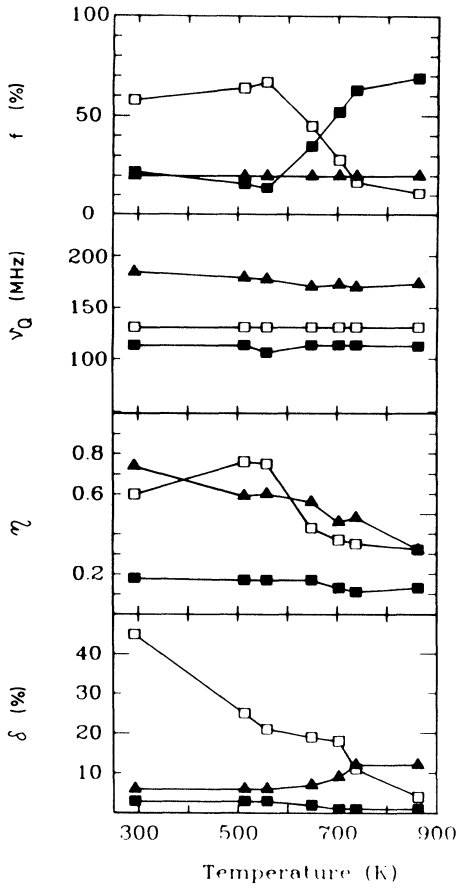

FIG. 6. Values of the hyperfine parameters as a function of the measurement temperature T_m. The symbols ■, □, and ▲ correspond to the interactions labeled I_1, I_2, and I_3, respectively.

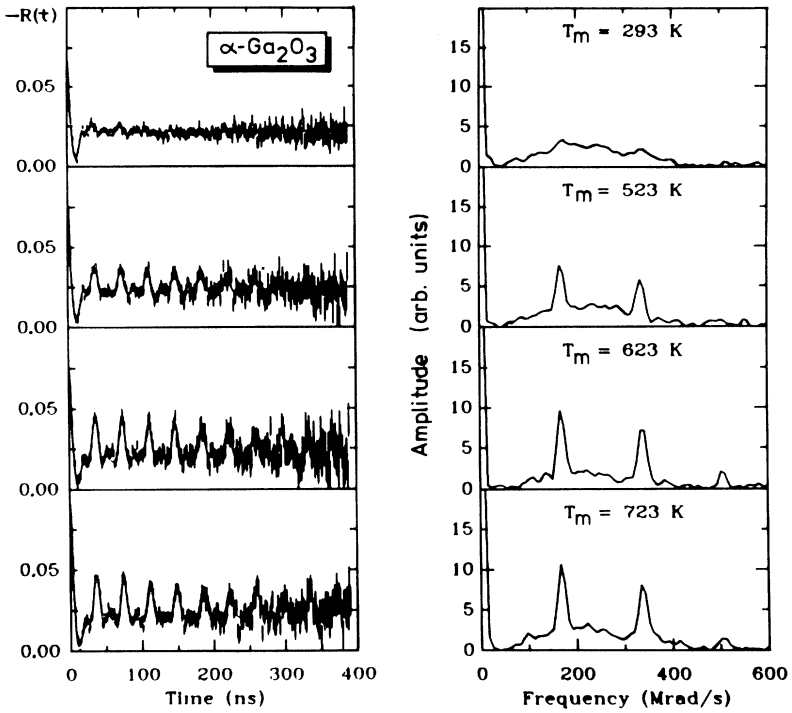

FIG. 7. PAC spectra and their Fourier transforms for ^{111}Cd in polycrystalline α-Ga_2O_3 obtained as function of the measurement temperature.

^{111}In probes are likely to occupy undisturbed cation sites after the annealing procedure. In α-Ga_2O_3 only *one* site exists having sixfold oxygen coordination, whereas in β-Ga_2O_3 *two* different sites with *either* octahedral *or* tetrahedral oxygen coordination exist.

Therefore, care has to be taken in correlating the observed hyperfine interactions with the different sites in β-Ga_2O_3. We follow two lines of argumentation: First we compare our data with that on bixbyite In_2O_3, having two octahedrally coordinated cation sites. Very recently, a simple correlation between the EFG's at these two sites with the radius of the cation was found.[2,22] The ionic radius of Ga^{3+} is the smallest one in this systematics and, unfortunately, Ga_2O_3 does not form a bixbyite phase. From this correlation we extrapolate a quadrupole coupling constant close to 180 MHz at the octahedral site of β-Ga_2O_3. Sesquioxides with smaller cations crystallize in the corundum structure as does α-Ga_2O_3. Systematic PAC experiments in corundum Al_2O_3,[7] Cr_2O_3,[23] Rh_2O_3,[24] and Ti_2O_3 (Ref. 25) gave $\nu_Q = 150 - 200$ MHz. In fact, the well-defined interaction I_1 in α-Ga_2O_3 having $\nu_Q = 180$ MHz would well fit to the systematics of corundum oxides.

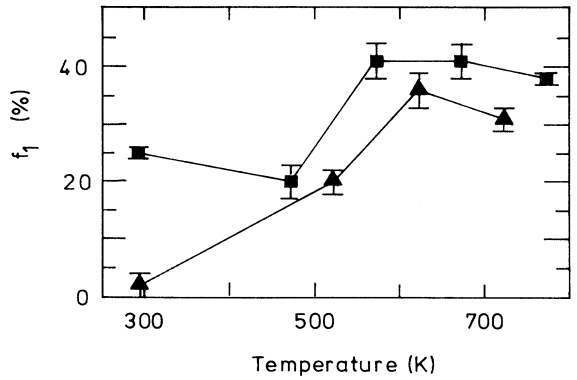

FIG. 8. Values of the fraction f_1 in α-Ga_2O_3 as a function of the measurement temperature. Measurements before (■) and after (▲) annealing at 773 K are distinguished.

This argumentation would suggest to correlate I_1 in α-Ga_2O_3 and I_3 in β-Ga_2O_3 with the *oxygen octahedra.*

In the second line of argumentation we use the spinel Mn_3O_4 for comparison[26] which has the same two cation coordinations as β-Ga_2O_3: an octahedrally and a tetrahedrally coordinated site. The ionic radii of Ga^{3+} and Mn^{3+} are nearly equal. The coupling constants for ^{111}Cd at the two sites in Mn_3O_4 have been determined:[26] $\nu_Q(\text{oct}) = 86.7$ MHz ($\eta = 0.13$) and $\nu_Q(\text{tet}) = 187$ MHz ($\eta = 0.89$), their ratio being $\nu_Q(\text{oct})/\nu_Q(\text{tet}) = 0.46$. Mössbauer experiments with ^{57}Fe in β-Ga_2O_3 have shown[27] that Fe^{3+} substitutes Ga^{3+} in the octahedral and tetrahedral sites. However, the sites are not occupied with the probabilities suggested by the lattice structure. Instead, it was found that approximately ten times as many iron atoms enter the octahedral site. The experimental quadrupole splittings Δ taken as a measure of the EFG's, give the ratio $\Delta(\text{oct})/\Delta(\text{tet}) = 0.525/0.98 = 0.54$. Assuming a similar behavior of In^{3+} and Fe^{3+}, we would expect a preferential occupation of the octahedral site in β-Ga_2O_3. In addition, the compound $InGaO_3$ has been reported as having the structure of β-Ga_2O_3, with In occupying again the octahedral site.[28]

With these observations we attribute the quadrupole coupling constant $\nu_Q(I_1, \beta\text{-}Ga_2O_3) = 120$ MHz to the *octahedral* site. The frequency $\nu_Q(I_3, \beta\text{-}Ga_2O_3) = 193$ MHz

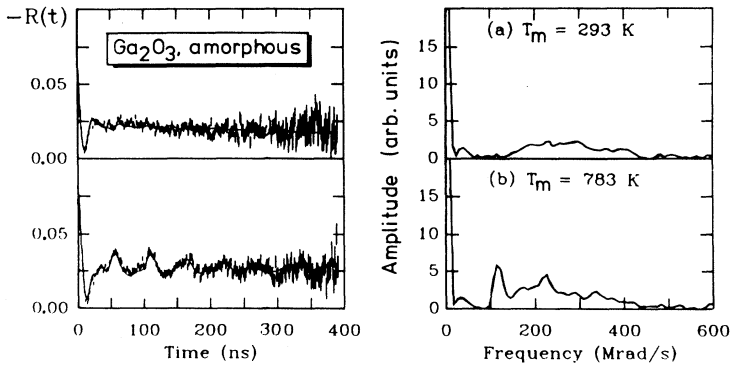

FIG. 9. PAC spectra and their Fourier transforms obtained with a sample of amorphous Ga_2O_3: (a) as-implanted, measured at room temperature; (b) after several annealings at temperatures below 783 K, measured at 783 K.

is likely to mark the tetrahedral site. This results in the frequency ratio $\nu_Q(\text{oct})/\nu_Q(\text{tet}) = 120/193 = 0.62$, close to the ratio of quadrupole splittings Δ mentioned before.

The smaller EFG at the octahedral site is easily understood in the point charge model (PCM): in the octahedron the average bond length $d(\text{In-O}) \approx 2$ Å is larger than in the tetrahedron, $d(\text{In-O}) = 1.85$ Å. To compare the absolute value of the EFG, we calculated the antishielding factor $\beta = 1 - \gamma = V_{zz}(\text{exp})/V_{zz}(\text{pcm}) = 36$ for the octahedral site. This value is in reasonable agreement with the standard value[29] for Cd, $\beta = 32.9$, and the systematics in ionic oxides[24]. The PCM predicts, however, for this site an asymmetry parameter of $\eta = 0.53$, in disagreement with the experimental value $\eta = 0.13 - 0.17$ which possibly points to small lattice distortions as found in TiO_2.[25]

For a final distinction between these two argumentations the single-crystal PAC data were evaluated. We denote the principal axes of the EFG tensor as xyz. If the γ rays are emitted along the principal axis of the EFG, their angular correlation is unperturbed. In Fig. 4 a high S_{20} value appears whenever the $\mathbf{e_3}$ crystallographic direction points to one of the detectors. It has to be concluded that the EFG principal component V_{zz} of interaction I_1 has this direction. In fact, point charge calculations (considering contributions of ions inside a sphere of 50 Å) predict that V_{zz} is along $\mathbf{e_3}$ for the octahedral site, but forms an angle of 8.8° with $\mathbf{e_3}$ for the tetrahedral coordinated site, as depicted in Fig. 10.

Although a small uncertainty remains due to the experimental uncertainty of the crystal orientation, we take this result as convincing enough to attribute the interaction I_1 to the octahedral site in β-Ga_2O_3. The discrepancy between the experimental EFG ($\nu_Q = 120$ MHz) and the one predicted from the scaling of the bixbyite oxides ($\nu_Q \approx 180$ MHz) may be explained by a contribution of covalent bonding as discussed by Wiarda *et al.*[27] for the case of Mn_2O_3 and β-Fe_2O_3. Furthermore, we conclude that in the case of β-Ga_2O_3 the sign of the electronic part of the EFG is opposite to the ionic one.

A final identification of the tetrahedral site still remains open. We prefer to assign the interaction I_3 in β-Ga_2O_3 to probe at the tetrahedral site, although the parameters of I_3 are quite similar for β-Ga_2O_3 *and* α-Ga_2O_3 and thus may indicate a similar origin. In the α phase no substitutional tetrahedral site exists.

B. Damping of the PAC spectra

The present PAC data on gallium oxides show an effect which occurs in several ^{111}In–doped ionic oxides of sixfold coordination: While the spectra taken at temperatures T_m above a critical temperature T_c exhibit well-defined EFG's, those taken below T_c are strongly damped. This effect is described for Y_2O_3 and other bixbyite oxides;[2,22] it was found in α-Fe_2O_3, ZrO_2, and In_2O_3 as well.[3,30,31] The damping can often be described by a Lorentzian or a Gaussian *static* frequency distribution. Whenever the "hard core" S_{20} is reduced below the value of a polycrystalline sample, the damping can only be explained by assuming the existence of *dynamical interactions*. In the case of the Ga oxides the attenuation at room temperature can be simply fitted with broad *static* frequency distributions while a dynamical interaction for the fractions I_1 and I_3 was only important near 500 K.

We have chosen the most naive description for the temperature dependence of fractions f_1 and f_2: the fraction f_1 of the well-defined interaction I_1 is rising at the expense of the broadly distributed interaction I_2. If we neglect the nearly constant component f_3 and renormalize the experimental fraction f_2 via $f_2^* = f_2/(f_1 + f_2)$, we obtain the f_2^* values displayed in Fig. 11, including the single-crystal results. As the next step we postulate the

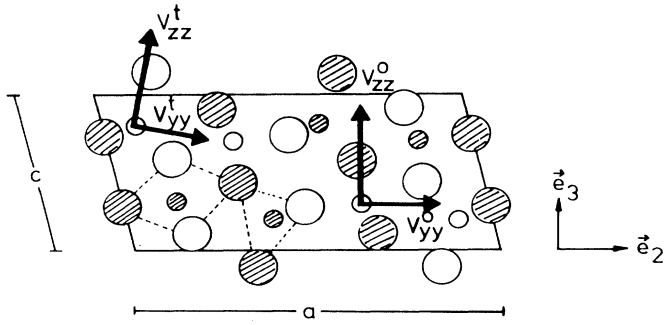

FIG. 10. The monoclinic unit cell of β-Ga_2O_3 seen along its b-axis. The smaller spheres mark the Ga ions. The hatched and unhatched ions are on different parallel planes, normal to the $\mathbf{e_1}$ direction and separated by the distance $b/2$. The EFG directions V_{zz} and V_{yy} for ^{111}Cd in a distorted oxygen octahedron (o) and in a distorted tetrahedron (t), respectively, are indicated, too.

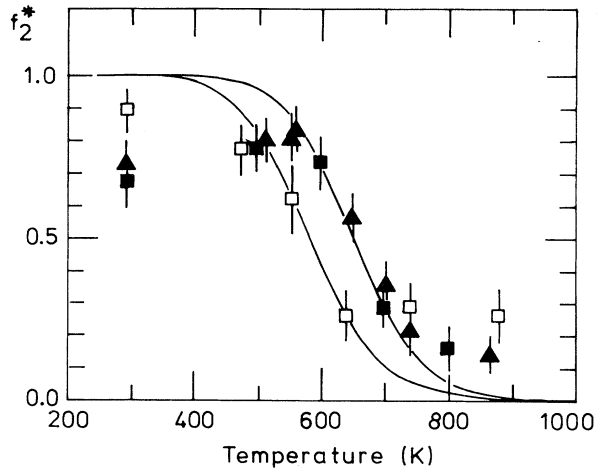

FIG. 11. Renormalized fraction f_2^* versus temperature. ■, vacuum; □, normal pressure; ▲, single-crystal results obtained at normal air pressure. The solid lines correspond to the concentration f^0 of neutral impurities calculated using the expression and parameters given in the Appendix.

existence of two charge states of the Cd impurity center: Cd^0 and Cd^-, the latter being responsible for the interaction I_1. The neutral Cd^0 center may consist of a Cd impurity atom with an electron hole bound to a neighboring oxygen ion. Such a localized hole would cause the interaction I_2 to have an EFG varying in magnitude and direction and therefore it would not produce a sharp undamped PAC pattern. Furthermore, the large distribution width δ_2 is attributed to small distortions at the center produced by the hole at the nonequivalent oxygen-ion sites. The present single-crystal measurements appear to support such an interpretation: At $T_m \geq 830$ K the EFG's of I_1 and I_2 have the same direction (see Fig. 4 and Table II). At room temperature — where the hole is bound — the "hard core" value S_{20} of the I_2 interaction has changed dramatically (see Fig. 12) indicating that the EFG no longer points in the $\mathbf{e_3}$ direction.

Looking for a source of such an electronic defect trapped to the center, we find as a possible origin the electron capture (EC) decay of ^{111}In.[2,3,32] PAC experiments using nuclear probes which decay by β or γ emission do not show this damping of the perturbation function below T_c. This was proven by measurements in some bixbyite oxides after implanting ^{111m}Cd,[2] where the same PAC-sensitive level is populated via γ emission. Furthermore, PAC experiments with the β-decaying ^{181}Hf probe in the same β-Ga_2O_3 crystal did not show any changes of the spectra at T_c,[33] nor did the Mössbauer spectra of Fe-doped β-Ga_2O_3 change between 80 and 1000 K.[15] We conclude that in the present experiments the Cd^0 charge state of the center is connected with the EC decay of ^{111}In.

Finally we try to understand the transition from I_2 to I_1 at T_c. The large energy gap of β-Ga_2O_3 prevents intrinsic semiconduction. Another possibility is the thermal ionization of the Cd acceptor center: $Cd^0 \leftrightarrow Cd^- + h^+$. In the Appendix the fraction f^0 of neutral impurities at temperature T is estimated within this two-state model. In Fig. 11 the solid lines are the calculated f^0 curves, using the values of the ionization energy and the acceptor concentration estimated in the Appendix. Obviously, the calculation reproduces the general trend of f_2^*, but fails in reproducing the asymptotic values. We finally note the difference of the f_2^* curves taken at different oxygen pressures which evidently is connected with a reduction of the ionization energy and an increase of the concentration of ionizable defects. In order to more clearly investigate the influence of the oxygen pressure, one would have to vary this parameter over a much larger range.

C. Other forms of Ga_2O_3

The α form of Ga_2O_3 with corundum structure has already been discussed in Sec. V A. The interaction I_1 was attributed to substitutional ^{111}Cd on the octahedrally coordinated cation site. We add here the results of the PCM calculation for this phase. The calculated antishielding factor, $\beta = 83$, is in good agreement with the corundum systematics[24] and the calculated asymmetry parameter $\eta = 0$ agrees with the experimental one. The α form exhibits a damping with the critical temperature $T_c \approx 580$ K (see Fig. 8). In analogy to β-Ga_2O_3 we interpret the interactions I_1 and I_2 as charged Cd^- (I_1) and neutral Cd^0 probes (I_2). In many oxides broad frequency distributions centered around the first harmonics of the substitutional fraction[1] have been observed which

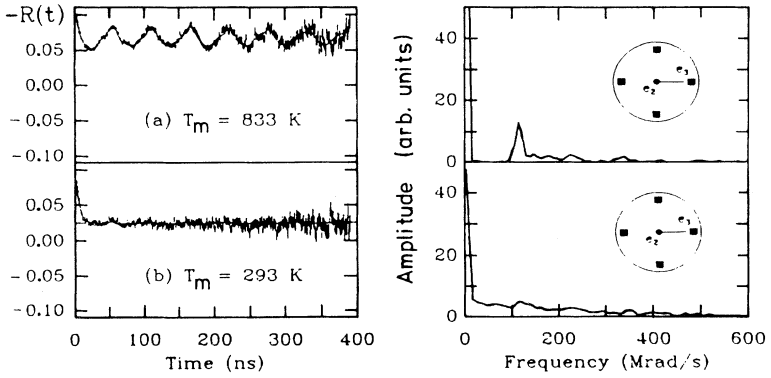

FIG. 12. PAC spectra and their Fourier transforms in the β-Ga_2O_3 crystal, taken at different measuring temperatures T_m without changing the positions either of the crystal or the detectors. The insets are used as in Fig. 4.

are usually assigned to probes on substitutional sites in a somewhat imperfect lattice. In the present case we propose this interpretation for the interaction I_3 in α-Ga_2O_3, too, but recall the observation of a similar interaction in β-Ga_2O_3. After annealing the PAC spectra showed the dominating interaction I_1 of β-Ga_2O_3, indicating that the phase transition from the α form to the β form has taken place according to Fig. 1. Likewise, amorphous Ga_2O_3 was transformed into the β form as predicted in the schema of Fig. 1. As all samples were checked by x-ray analysis, we take these phase transitions to occur at the right conditions as an additional proof for our site attribution.

VI. CONCLUSIONS

We have studied the hyperfine interactions of ^{111}Cd in different forms of gallium oxide following the implantation of radioactive ^{111}In tracers. In all samples we found the existence of several hyperfine environments. The most important conclusions can be summarized as follows.

(1) The characteristic electric quadrupole interaction(s) in each phase were seen best at high measuring temperatures $T_m \geq 700$ K, whereas broadly distributed interactions dominate the PAC spectra at moderate temperatures and lead to strongly damped perturbation patterns.

(2) In β-Ga_2O_3 ^{111}In (implanted or diffused) prefers the sixfold coordinated (octahedral) site. This assignment is based on the temperature dependence of the hyperfine interaction and single-crystal measurements. Point charge calculations predict a more asymmetric EFG at this site.

(3) The temperature dependence of the hyperfine interactions is explained by assuming two configurations for substitutional Cd in α- and β-Ga_2O_3. One corresponds to ionized Cd^- on a normal cation site. The other one corresponds to neutral Cd^0 with an electronic hole possibly localized in a neighboring oxygen ion.

ACKNOWLEDGMENTS

This work has been partly supported by the Stiftung Volkswagenwerk (Germany). One of us (A.F.P.) acknowledges the support of CONICET and CICPBA (Argentina). We cordially thank Professor W. Gunsser, Universität Hamburg, who supplied the β-Ga_2O_3 single crystals used in this study.

APPENDIX: DEFECT IONIZATION IN SEMICONDUCTORS

To describe the transition from I_2 to I_1 we will calculate the number f^0 of neutral impurities Cd^0 at a given temperature T. This number f^0 has then to be compared with the renormalized PAC fraction f_2^*. We assume only one type of defect which should be acceptors. Writing for the ionization

$$A^- + h^+ \leftrightarrow A^0, \tag{A1}$$

we can apply the mass action law as

$$n^2/(N_A - n) = K \tag{A2}$$

since the concentrations $[A^-] = [h^+] = n$ and $[A^0] = N_A - n$. From thermodynamical considerations,[34] the constant K is given by

$$K = (2m\pi kT/h^2)^{3/2} \exp(-\epsilon/kT). \tag{A3}$$

Here ϵ is the ionization energy. With the definitions $x = \epsilon/kT$, and $b = (N_A)^{2/3}h^2/2m\pi\epsilon$ the probability of the defect being neutral is

$$f^0 = [v - \sqrt{(v^2+1)}\ ]^2, \tag{A4}$$

where $v = 0.5 \cdot (bx)^{-3/4} \exp(-x/2)$.

The ionization energy ϵ and the acceptor concentration N_A can be obtained from Eq. (A4) if two v values are known as a function of T. If they are v_1 and v_2 at T_1 and T_2, we can write

$$\epsilon = k \left(\frac{1}{T_1} - \frac{1}{T_2}\right)^{-1} \left[2 \ln\left(\frac{v_2}{v_1}\right) + \frac{3}{2} \ln\left(\frac{T_1}{T_2}\right)\right] \tag{A5}$$

and then N_A can be evaluated from b.

The experimental results given in Fig. 11 are described by this reaction mechanism $Cd^0 \leftrightarrow Cd^- + h^+$, the curves in the figure have been calculated to pass two points in the transition zone using the following values for the ionization energy and impurity concentration: $\epsilon = 0.96$ eV and $N_A = 2.9 \times 10^{12}$ cm^{-3} at normal oxygen pressure and $\epsilon = 0.72$ eV and $N_A = 3.7 \times 10^{13}$ cm^{-3} at low pressure (2×10^{-5} mbar). If one takes the errors of the data into account we can only estimate an ionization energy of about 1 eV and an impurity concentration in the range from 10^{12} cm^{-3} to 10^{13} cm^{-3}.

[1] W. Bolse, M. Uhrmacher, and K.P. Lieb, Phys. Rev. B **36**, 1818 (1987); W. Bolse, M. Uhrmacher, A. Bartos, J. Kesten, and K.P. Lieb, Ber. Bunsenges. Phys. Chem. **93**, 1253 (1989).

[2] A. Bartos, K.P. Lieb, A.F. Pasquevich, and M. Uhrmacher, Phys. Lett. A **157**, 513 (1991); A. Bartos, K.P. Lieb, M. Uhrmacher, and D. Wiarda, Acta Crystallogr. B **49**, 165 (1993).

[3] A.G. Bibiloni, C.P. Massolo, J. Desimoni, L.A. Mendoza-Zélis, F.H. Sanchez, A.F. Pasquevich, L. Damonte, and A.R. Lopez-Garcia, Phys. Rev. B **32**, 2393 (1985).

[4] Th. Wichert, N. Achtziger, H. Metzner, and R. Sielemann, in *Hyperfine Interactions of Defects in Semiconductors*, edited by G. Langouche (Elsevier, Amsterdam, 1992), p. 79ff, and references therein; A.F. Pasquevich and R. Vianden, Phys. Rev. B **41**, 10 956 (1990).

[5]A.F. Pasquevich, Hyperfine Interact. **60**, 791 (1990).
[6]C.W. White, L.A. Boatner, P.S. Sklad, C.J. McHargue, J. Rankin, G.C. Farlow, and M.J. Aziz, Nucl. Instrum. Methods B **32**, 11 (1988).
[7]J. Kesten, Hyperfine Interact. **52**, 17 (1989).
[8]J.C. Austin, M.L. Swanson, W.C. Hughes, C.T. Kao, L.M. Slifkin, H.C. Hofsäss, and E.C. Frey, Phys. Rev. B **42**, 7699 (1990).
[9]D. Wegner, Hyperfine Interact. **23**, 179 (1985).
[10]N.N. Greenwood and A. Earnshaw, *Chemistry of the Elements* (Pergamon, New York, 1963), p. 278.
[11]S. Geller, J. Chem. Phys. **33**, 6766 (1960).
[12]Hyung-Gon Kim and Wha-Tek Kim, J. Appl. Phys. **62**, 2000 (1987).
[13]H.H. Tippins, Phys. Rev. **137**, 865 (1965).
[14]R. Büscher and G. Lehmann, Z. Naturforsch. Teil A **42**, 67 (1987).
[15]J.M. Trooster and A. Dymanus, Phys. Status Solidi **24**, 487 (1967).
[16]R.W.G. Wyckoff, *Crystal Structures* (Interscience, New York, 1969).
[17]G. Harms, Diploma thesis, Hamburg, 1975 (unpublished).
[18]M. Uhrmacher, K. Pampus, F.J. Bergmeister, D. Purschke, and K.P. Lieb, Nucl. Instrum. Methods. B **9**, 234 (1985).
[19]H. Schroeder, W. Bolse, M. Uhrmacher, and K.P. Lieb, Z. Phys. B **65**, 193 (1986).
[20]L.A. Mendoza-Zélis, A.G. Bibiloni, M.C. Caracoche, A.R. Lopez-Garcia, J.A. Martinez, R.C. Mercader, and A.F. Pasquevich, Hyperfine Interact. **3**, 315 (1977).
[21]A. Baudry, P. Boyer, and A.L. de Oliveira, Hyperfine Interact. **10**, 1003 (1981).
[22]J. Shitu, D. Wiarda, T. Wenzel, M. Uhrmacher, K.P. Lieb, S. Bedi, and A. Bartos, Phys. Rev. B **46**, 7987 (1992).
[23]J. Kesten, M. Uhrmacher, and K.P. Lieb, Hyperfine Interact. **59**, 309 (1990).
[24]J. Kesten, W. Bolse, K.P. Lieb, and M. Uhrmacher, Hyperfine Interact. **60**, 683 (1990); D. Wiarda, M. Uhrmacher, A. Bartos, and K.P. Lieb, J. Phys.: Condens. Matter **5**, 4111 (1993).
[25]Th. Wenzel, A. Bartos, K.P. Lieb, M. Uhrmacher, and D. Wiarda, Ann. Phys. **1**, 155 (1992).
[26]D. Wiarda, A. Bartos, K.P. Lieb, M. Uhrmacher, and Th. Wenzel, in *Proceedings of the XXV Zakopane School on Physics,* edited by J. Stanek (World Scientific, Singapore, 1990) Vol. 1, p. 340; D. Wiarda, Th. Wenzel, M. Uhrmacher, and K.P. Lieb, J. Phys. Chem. Solids **53**, 1199 (1992).
[27]S. Geschwind, Phys. Rev. **121**, 363 (1961).
[28]J.B. Goodenough, J.A. Kafalas, and J.M. Longo, in *Preparative Methods in Solid State Chemistry*, edited by P. Hagemuller (Academic, London, 1972), p. 14.
[29]N.C. Mahapatra, P.C. Pattnaik, M.D. Thompson, and T.P. Das, Phys. Rev. B **16**, 3001 (1977).
[30]K. Asai, F. Ambe, S. Ambe, T. Okada, and H. Sekizawa, Phys. Rev. B **41**, 6124 (1990).
[31]W.E. Evensen, A.G. McKale, H.T. Su, and J.A. Gardner, Hyperfine Interact. **61**, 1379 (1990).
[32]U. Bäverstam, R. Othaz, N. de Sousa, and B. Ringström, Nucl. Phys. **A186**, 500 (1972).
[33]J. Shitu and A.F. Pasquevich (unpublished).
[34]G.I. Pearson and J. Bardeen, Phys. Rev. **75**, 865 (1949).